THE JOURNAL OF PHYSICAL CHEMISTRY B

ARTICLE

pubs.acs.org/JPCB

Reaction Pathway and Free Energy Profile for Butyrylcholinesterase-Catalyzed Hydrolysis of Acetylcholine

Xi Chen,[§,†,‡] Lei Fang,[§,‡] Junjun Liu,[‡] and Chang-Guo Zhan[‡,*]

[†]Key Laboratory of Pesticide & Chemical Biology of the Ministry of Education, College of Chemistry, Central China Normal University, Wuhan 430079, P. R. China

[‡]Department of Pharmaceutical Sciences, College of Pharmacy, University of Kentucky, 789 South Limestone Street, Lexington, Kentucky 40536, United States

ABSTRACT: A catalytic mechanism for the butyrylcholinesterase (BChE)-catalyzed hydrolysis of acetylcholine (ACh) has been studied by performing pseudobond first-principles quantum mechanical/molecular mechanical-free energy calculations on both acylation and deacylation of BChE. It has been shown that the acylation with ACh includes two reaction steps, including nucleophilic attack on the carbonyl carbon of ACh and dissociation of choline ester. The deacylation stage includes nucleophilic attack of a water molecule on the carboxyl carbon of the substrate and dissociation between the carboxyl carbon of the substrate and the hydroxyl oxygen of the Ser198 side chain. Notably, despite the fact that acetylcholinesterase (AChE) and BChE are very similar enzymes, the acylation of BChE with ACh is rate-determining, which is remarkably different from the AChE-catalyzed hydrolysis of ACh, in which the deacylation is rate-determining. The computational prediction is consistent with available experimental kinetic data. The overall free energy barrier calculated for BChE-catalyzed hydrolysis of ACh is 13.8 kcal/mol, which is in good agreement with the experimentally derived activation free energy of 13.3 kcal/mol.

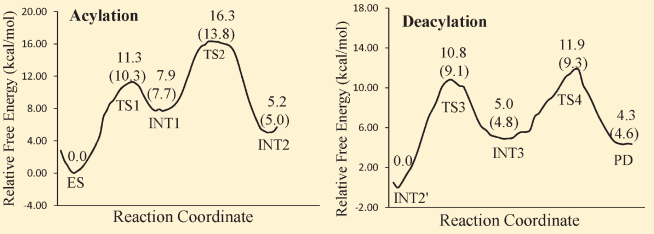

INTRODUCTION

Cholinesterases are a family of enzymes that catalyze the hydrolysis of neurotransmitter acetylcholine (ACh), an essential reaction necessary to allow a cholinergic neuron to return to the resting state after impulse transmission. There are two types of cholinesterases, acetylcholinesterase (AChE) and butyrylcholinesterase (BChE), which differ in their distribution in the body. AChE exists mainly in neuromuscular junctions and cholinergic synapses and hydrolyzes ACh with extremely high efficiency.[1] BChE is known as plasma cholinesterase, which is widely distributed in tissues and plasma. Although the physiological roles of BChE are still not completely clear, it has been found that BChE can catalyze the hydrolyses of various acyl cholines, acyl thiocholines,[2] cocaine,[3] and acetanilides.[4] It has been noted that BChE can rapidly hydrolyze ACh in the nerves and brain,[5,6] and thus, BChE can apparently substitute for AChE in maintaining the structural and functional integrity of central cholinergic pathways.

In addition, BChE has been proven a therapeutically important protein. First of all, BChE has been clinically used as a bioscavenger for detoxification of organophosphorus (OP) nerve agents.[7,8] Our recently reported studies[3,9−22] have led to the discovery of high-activity mutants of BChE with a considerably improved catalytic efficiency against naturally occurring, widely abused cocaine. The high-activity mutants of BChE have been recognized as promising candidates for therapeutic treatment of cocaine overdose and addiction.[23] In addition, BChE is an important target for cholinergic drugs (that include reversible inhibitors of BChE, AChE, or both) in treatment of Alzheimer disease, etc.[24]

According to the X-ray crystal structures of AChE and BChE reported so far, the overall architecture of BChE is quite similar to that of AChE.[25] The active site of BChE is located at the bottom of a deep "aromatic gorge" lined by side chains of several aromatic residues. The channel leading from the surface to the active site is much less confining than that of AChE;[26] hence, the active site of BChE can accommodate larger ligands, such as cocaine.[10] Similar to that in AChE, the active site of BChE possesses a catalytic triad (consisting of Ser198, Glu325, and His438) and an oxyanion hole (consisting of Gly116, Gly117, and Ala199) that are essential for the catalytic function. It is commonly accepted that when a substrate reaches the active site of BChE, the hydroxyl group of Ser198 acts as a nucleophile to attack the carbonyl carbon of the substrate, which initiates the acylation of BChE. The acylation gives an acyl−enzyme intermediate. Subsequently, a water molecule initiates the deacylation to break the ester linkage (Scheme 1). Throughout the hydrolysis process, the Glu325−His438 pair is crucial in activating the nucleophile and in transferring a proton to the leaving group and, thus, significantly accelerates the hydrolysis reaction.

Received: November 9, 2010
Revised: December 7, 2010
Published: December 22, 2010

Scheme 1. Proposed Catalytic Reaction Pathway for BChE-Catalyzed Hydrolysis of Acetylcholine[a]

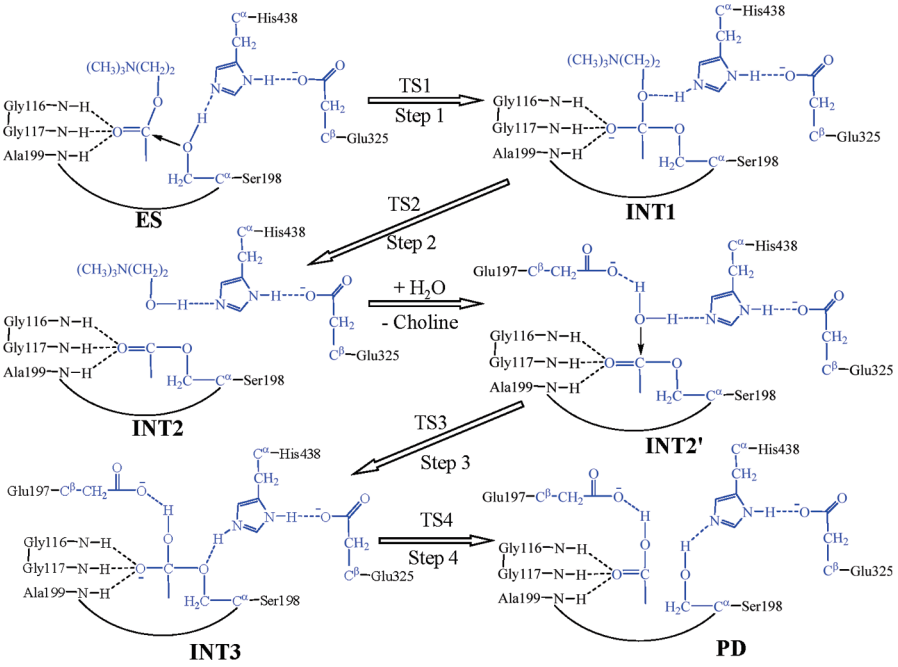

[a] Atoms colored in blue are treated by the QM method in the pseudobond first-principles QM/MM calculations. Three boundary carbon atoms (C^{α} or C^{β}) are treated with the improved pseudobond parameters.[39] All other atoms belong to the MM subsystem.

Cholinesterase-catalyzed hydrolysis of ACh has been the topic for extensive experimental and computational studies.[1,27−38] Kinetic study[37] has revealed that the reaction rate constant for the deacylation is smaller than that for the acylation, indicating that the deacylation is rate-determining for AChE-catalyzed hydrolysis of ACh. Reported QM/MM studies[36,38] on AChE-catalyzed hydrolysis of ACh has further suggested that the first reaction step in deacylation is rate-determining for the catalytic hydrolysis process.

Despite extensive computational studies on the catalytic mechanisms of AChE,[1,15,27−30,33,34,36,38] the detailed reaction mechanism for the BChE-catalyzed hydrolysis of ACh still remains to be examined. On the basis of the high similarity between AChE and BChE structures, it seems to be reasonable to assume that the catalytic mechanism for the BChE-catalyzed hydrolysis of ACh is the same as that for the AChE-catalyzed hydrolysis of ACh. However, to our surprise, the present study has demonstrated that the reaction mechanism for the BChE-catalyzed hydrolysis of ACh is remarkably different from the well-known mechanism for the AChE-catalyzed hydrolysis of ACh in terms of the rate-determining reaction step.

In the present study, we have carried out pseudobond first-principles quantum mechanical/molecular mechanical-free energy (QM/MM-FE) calculations[39−42] to study the detailed reaction pathways for the BChE-catalyzed hydrolysis of ACh. The pseudobond first-principles QM/MM-FE approach[39,40,42,43] has been demonstrated to be a powerful tool in simulating a variety of enzymes,[12,30,41,44−46] and some theoretical predictions[30,46] were subsequently confirmed by experimental studies.[47−49] The computational data clearly reveal the detailed reaction pathway and the corresponding free energy profiles for the BChE-catalyzed hydrolysis of ACh. The rate-determining step is thereby identified, and the roles of essential residues, including the catalytic triad and oxyanion hole, are discussed on the basis of the QM/MM-optimized geometries of key states in each catalytic hydrolysis reaction process.

COMPUTATIONAL AND EXPERIMENTAL METHODS

Preparation of the Initial Structures. The X-ray crystal structure of BChE (PDB ID: 1P0M)[50] and the structure of ACh in its fully extended conformation[30] were used to construct the initial Michaelis−Menten complex structure of BChE-ACh complex (ES in Scheme 1). The water molecules in the active site and the choline molecule in the BChE crystal structure were removed from the BChE crystal structure. In the initial complex structure, the carbonyl oxygen of ACh was placed in the oxyanion hole consisting of Gly116, Gly117, and Ala199, and the positively charged $-N-(CH_3)_3$ moiety of ACh was placed close to the choline binding site nearby Trp82.[36,50] The molecular geometry of ACh was optimized by performing ab initio quantum chemical calculations using the Gaussian03 program[51] at the HF/6-31G* level. The optimized geometry was used to calculate the electrostatic potential on the molecular surface at the same HF/6-31G* level. The calculated electrostatic potential was used to determine partial atomic charges with the standard restricted electrostatic potential (RESP) fitting procedure.[52,53] The determined RESP charges were used for the MD simulations. The constructed Michaelis−Menten complex was solvated in a rectangle box of TIP3P water molecules,[54] with a minimum solute wall distance of 10 Å. One chloride ion was added to neutralize the charge of the reaction system. As seen in Scheme 1, there are two stages in the BChE-catalyzed hydrolysis of ACh. The choline leaves the system after acylation. Consequently, we constructed the structure of INT2′ by removing the choline from the QM/MM-optimized INT2 structure. The constructed INT2′ structure was then relaxed by performing ~2 ns of MD simulation in which the system was also solvated in a rectangle box with

TIP3P water molecules,[54] with a minimum solute wall distance of 10 Å.

For both acylation and deacylation stages, the last snapshots of MD simulations were used to prepare the pseudobond first-principles QM/MM calculations because the structure of the last snapshot was close to the average structure simulated. Since we are interested in the reaction center, the water molecules beyond 50 Å of the carbonyl carbon of ACh were removed, leaving the QM/MM system with 3022 water molecules and a total of 17 457 atoms for the acylation stage, and 2993 water molecules and a total of 17 348 atoms for the deacylation stage. The QM/MM interface was dealt with by using a pseudobond approach.[39,40,43] The used boundary of the QM/MM system for both stages is depicted in Scheme 1. Prior to the QM/MM geometry optimizations, each initial reaction system was energy-minimized with the MM method by using the revised AMBER8 program,[55] in which the convergence criterion is a root-mean-square deviation (rmsd) of the energy gradient of less than 0.1 kcal·mol^{-1}·Å^{-1}.

Minimum-Energy Path of the Enzymatic Reaction. With a reaction coordinate driving method and an iterative energy minimization procedure,[42] the enzyme reaction path was determined by the pseudobond QM/MM calculations at the B3LYP/6-31G*:AMBER level, in which the QM calculations were performed at the B3LYP/6-31G* level of theory by using a modified version of the Gaussian03 program,[51] and the MM calculations were performed by using a modified version of the AMBER8 program.[55] Normal mode analyses were performed to characterize the reactants, intermediates, transition sates, and final products. In addition, single-point energy calculations were carried out at the QM/MM(MP2/6-31+G*:AMBER) level on the QM/MM-optimized geometries. Throughout the QM/MM calculations, the boundary carbon atoms were treated with improved pseudobond parameters.[39] No cutoff for nonbonded interactions was used in the QM/MM calculations. For the QM subsystem, the convergence criterion for geometry optimizations follows the original Gaussian03 defaults. For the MM subsystem, the geometry optimization convergence criterion is when the root-mean-square deviation of energy gradient is <0.1 kcal·mol^{-1}·Å^{-1}. Prior to QM/MM calculations, the MM subsystem was relaxed by performing ~500 steps of energy minimization with the AMBER8 program. Then atoms within 20 Å of the carbonyl carbon (C1) of ACh were allowed to move while all the other atoms outside this range were frozen in all QM/MM calculations.

Free Energy Perturbation. After the minimum-energy path was determined by the QM/MM calculations, the free energy changes associated with the QM/MM interactions were determined by using the free energy perturbation (FEP) method.[42] In the FEP calculations, sampling of the MM subsystem was carried out with the QM subsystem frozen at different states along the reaction path. The point charges on the frozen QM atoms used in the FEP calculations were those determined by fitting the electrostatic potential (ESP) for the QM part of the QM/MM single-point calculations. The total free energy difference between the transition state and the reactant was calculated with the same procedure used in our previous work on other reaction systems.[44] The FEP calculations enabled us to more reasonably determine relative free energy changes due to the QM/MM interaction. Technically, the final (relative) free energy determined by the QM/MM-FE calculations is the QM part of the QM/MM energy (excluding the Coulombic interaction energy between the point charges of the MM atoms and the ESP charges of the QM atoms) plus the relative free energy change determined by the FEP calculations. In the FEP calculations, the time step used was 2 fs, and bond lengths involving hydrogen atoms were constrained. In sampling of the MM subsystem by MD simulations, the temperature was maintained at 298.15 K. Each FEP calculation consisted of 50 ps of equilibration and 300 ps of sampling.

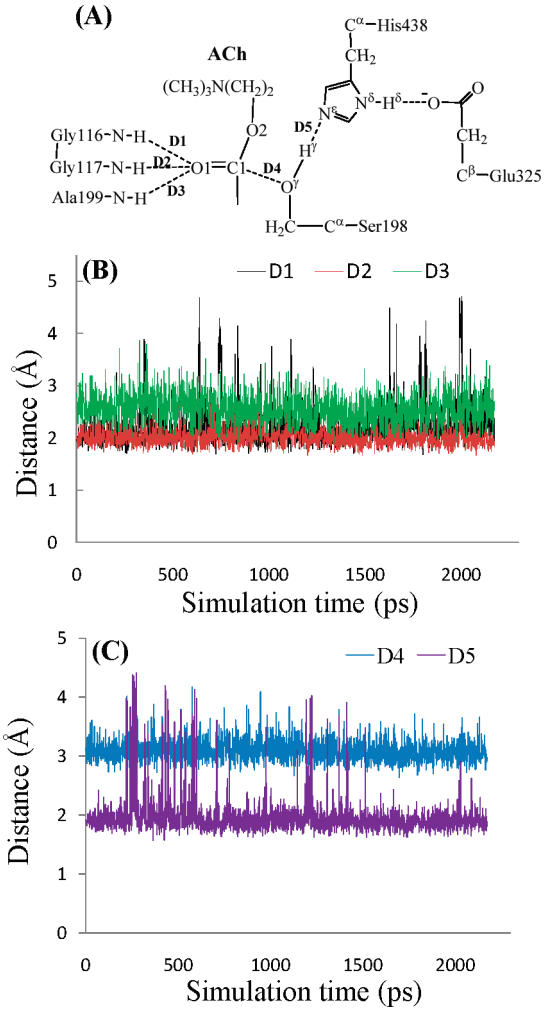

Figure 1. Key internuclear distances (D1−D5) vs simulation time in the MD-simulated BChE−ACh complex.

The MD simulations and QM/MM-FE calculations were performed on a supercomputer (e.g., IBM X-series cluster with 340 nodes or 1360 processors) at the University of Kentucky Center for Computational Sciences. The other modeling and computations were carried out on SGI Fuel workstations and a 34-processor IBM x335 Linux cluster in our own laboratory.

RESULTS AND DISCUSSION

BChE-ACh Binding Structure from MD Simulation. We performed ~2 ns MD simulation on the BChE-ACh complex to study the enzyme−substrate (ES) binding. Collected in Figure 1 are plots of key internuclear distances vs simulation time in the MD-simulated ES complex. Traces D1, D2, and D3 represent the internuclear distances between the carbonyl oxygen O1 of ACh and the NH hydrogen atoms of residues Gly116, Gly117, and

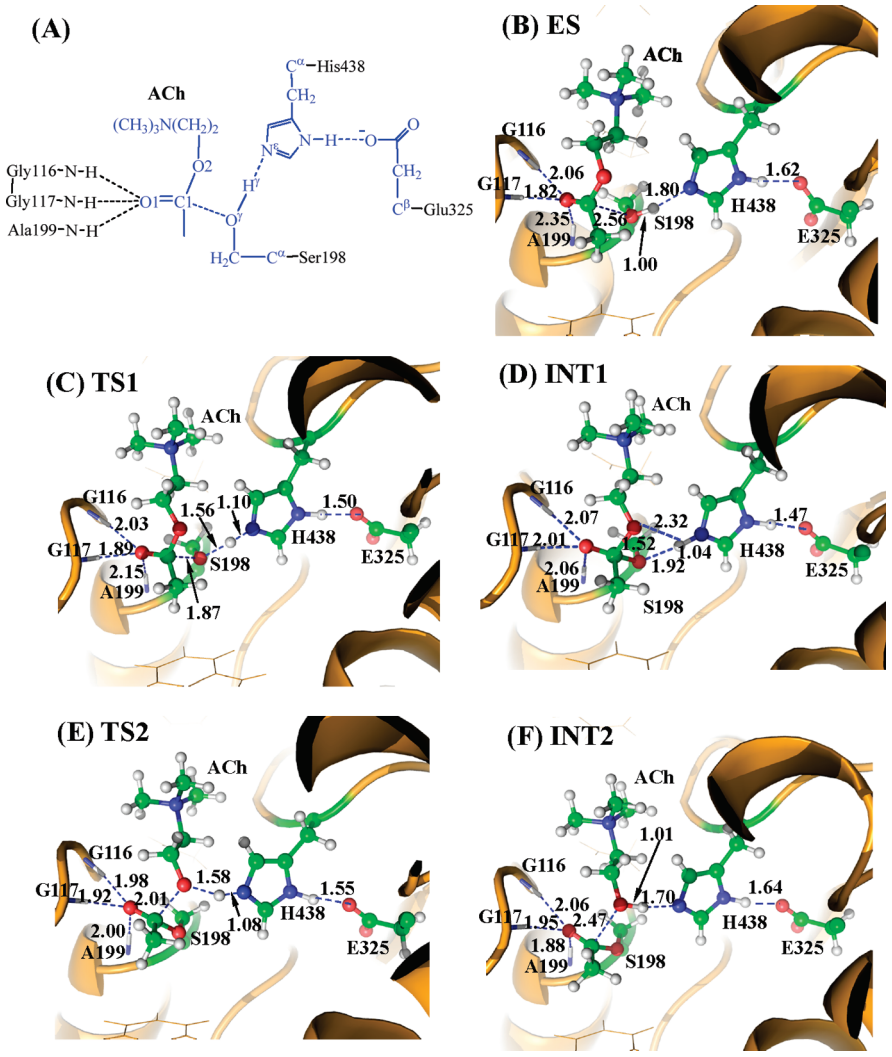

Figure 2. Key states for the acylation reaction stage of BChE-catalyzed ACh hydrolysis. The geometries were optimized at the QM/MM(B3LYP/6-31G*:AMBER) level. The key distances in the figure are in angstroms. Carbon, oxygen, nitrogen, and hydrogen atoms are green, red, blue, and white, respectively. The backbone of the protein is orange. The QM atoms are represented as balls and sticks, and the surrounding residues are rendered as sticks or lines. The figures below are represented using the same method.

Ala199, respectively. Trace D4 is the internuclear distance between the hydroxyl oxygen (O^{γ}) of the Ser198 side chain and the carbonyl carbon C1 of ACh. Trace D5 is the internuclear distance between the hydroxyl hydrogen (H^{γ}) of the Ser198 side chain and the N^{ε} atom of the His438 side chain.

As seen in Figure 1B, in the MD-simulated ES complex, the average values of D1, D2, and D3 are ~2.1, ~2.2, and ~2.7 Å, respectively, showing that the carbonyl oxygen O1 of ACh forms two hydrogen bonds with the oxyanion hole formed by the backbone NH groups of Gly116, Gly117, and Ala199. The average value of D4 in Figure 1C is ~3.1 Å, indicating an appropriate distance for the Ser198 hydroxyl to start nucleophilic attack on the carbonyl carbon C1 of ACh. The average value of D5 is ~2.0 Å, suggesting that His438, the general base in the BChE catalytic triad, has been positioned well and is ready for facilitating the nucleophilic attack process through accepting a proton from the nucleophile.

Fundamental Reaction Pathway for BChE-Catalyzed Hydrolysis of ACh. The MD simulation led to a dynamically stable ES complex. Our QM/MM reaction coordinate calculations at the B3LYP/6-31G*:AMBER level starting from the MD-simulated ES complex revealed that the BChE-catalyzed hydrolysis of ACh consists of four reaction steps. The first step is the nucleophilic attack on the carbonyl carbon C1 of ACh by the O^{γ} atom in Ser198. The second reaction step is the dissociation between the acetyl group and the choline of ACh. The third reaction step is the nucleophilic attack on the carboxyl carbon of acylated Ser198 by a water molecule. The fourth reaction step is the dissociation between the acetyl group and Ser198 of BChE. The optimized geometries of the reactant, intermediates, transition states, and final product are shown in Figure 2. We will discuss each of these reaction steps in detail.

Step 1: Nucleophilic Attack on the Carbonyl Carbon C1 by the O^{γ} Atom of Ser198. Before studying the reaction pathway, the ES complex structure was first optimized at the QM/MM-(B3LYP/6-31G*:AMBER) level. As shown in Figure 2B, the QM/MM-optimized geometrical parameters D1, D2, D3, and D4 (refer to Figure 1A) are 2.06, 1.82, 2.35, and 2.56 Å, respectively. It has been shown that the corresponding values of D1−D4 in the calculated AChE−ACh Michaelis−Menten

dx.doi.org/10.1021/jp110709a |J. Phys. Chem. B 2011, 115, 1315–1322

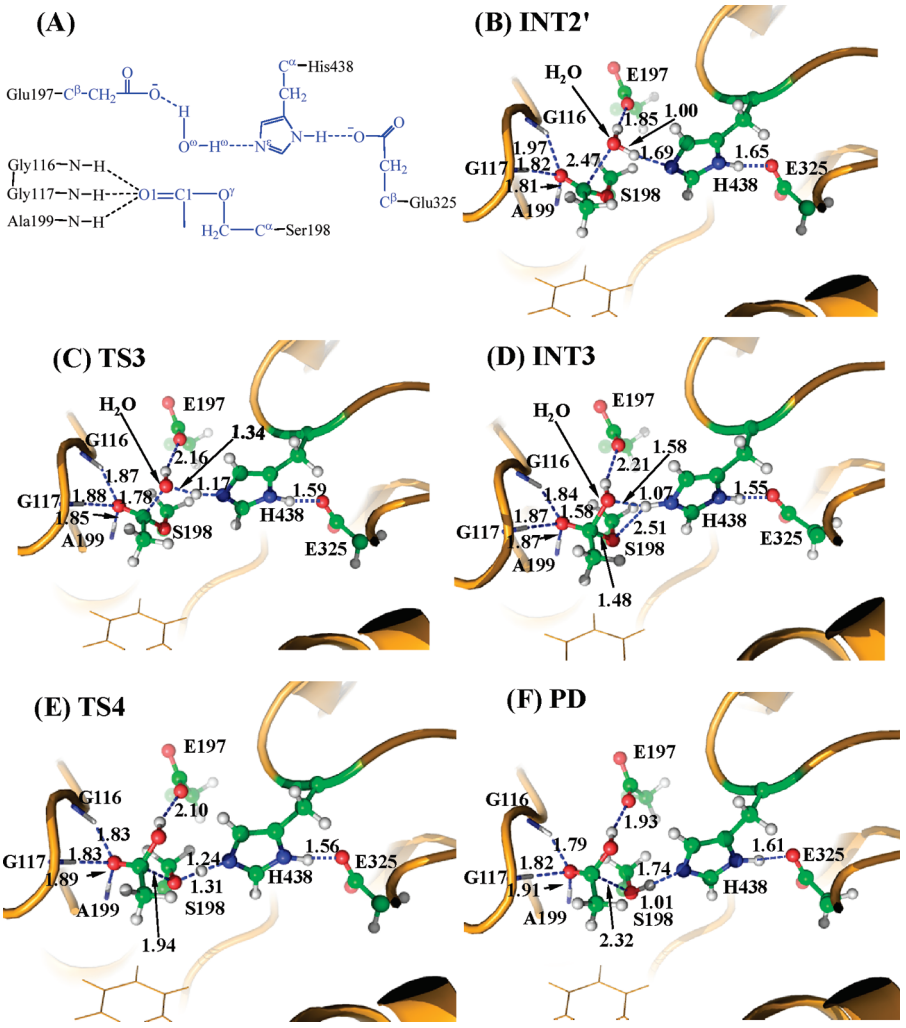

Figure 3. Key states for the deacylation reaction of BChE-catalyzed ACh hydrolysis. The geometries were optimized at the QM/MM(B3LYP/6-31G*:AMBER) level. See the caption of Figure 2 for the color codes for the different types of atoms.

complex[30,36] were estimated to be 1.86, 1.82, 2.24, and 2.59 Å, respectively. The calculated values of D1−D3 reflect the binding of ACh with the oxyanion hole of BChE/AChE. Obviously, the binding of ACh with the oxyanion hole of BChE is slightly weaker than that of AChE.[36]

The nucleophilic attack process then proceeds as the hydroxyl oxygen O^{γ} of Ser198 gradually approaches the carbonyl carbon C1 of ACh. Meanwhile, the hydroxyl hydrogen, H^{γ}, of Ser198 gradually moves toward the nitrogen (N^{ε}) atom of the His438 side chain. Since this reaction step involves the breaking of the $O^{\gamma}-H^{\gamma}$ bond and the formation of both $C1-O^{\gamma}$ and $N^{\varepsilon}-H^{\gamma}$ bonds, as shown in Scheme 1, the distance between O^{γ} and H^{γ} ($R_{O\gamma-H\gamma}$), the distance between C1 and O^{γ} ($R_{C1-O\gamma}$), and the distance between N^{ε} and H^{γ} ($R_{N\varepsilon-H\gamma}$) reflect the nature of chemical reaction step 1. Therefore, the reaction coordinate for the current reaction step was set as $R_{O\gamma-H\gamma} - R_{C-O\gamma} - R_{N\varepsilon-H\gamma}$. As shown in the QM/MM-optimized geometries (Figure 2), when the O^{γ} atom of Ser198 gradually approaches the C1 atom, the geometry of the reactant (ES) in which the C1 atom is sp^2-hybridized and is in a planar geometry with its three attached groups gradually changes into a tetrahedral geometry centered at the sp^3-hybridized C1 atom in an intermediate (INT1) through a transition state (TS1).

Step 2: Dissociation of the Choline Ester. In this reaction step, the choline moiety of ACh gradually departs from the acetyl group in which the choline ester bond C1−O2 is broken. Meanwhile, the proton (H^{γ}) attached to the N^{ε} atom of the His438 side chain transfers to the choline oxygen atom (O2) of ACh. The changes in the distances R_{C1-O2}, $R_{O2-H\gamma}$, and $R_{N\varepsilon-H\gamma}$ reflect the nature of the dissociation process. Thus, the reaction coordinate for the current reaction step was chosen to be $R_{C1-O2} + R_{N\varepsilon-H\gamma} - R_{O2-H\gamma}$.

In the geometry of INT1, where the serine hydroxyl proton (H^{γ}) has been transferred to the N^{ε} atom of His438 in reaction step 1, the optimized distance ($R_{O\gamma-H\gamma}$) is 1.92 Å, suggesting the interaction between the Ser198 terminal oxygen and the protonated His438 side chain is weak. At the same time, the distance ($R_{O2-H\gamma}$) between H^{γ} and the leaving ester oxygen O2 to which H^{γ} is about to be transferred is 2.32 Å, indicating a weak hydrogen bond between the H^{γ} atom and the O2 atom. Hence, the H^{γ} atom is in the appropriate place to protonate the leaving O2 atom of ACh.

In changing from INT1 to TS2, there are two major types of structural changes. One is the gradual breaking of the covalent bond C1−O2 (R_{C1-O2} is 1.52 Å in INT1 and 2.01 Å in TS2). The other is the formation of a hydrogen bond ($N^{\varepsilon}-H^{\gamma}\cdots O2$)

indicated by the shorter and shorter distance $R_{O2-H\gamma}$ in going from INT1 to TS2 (2.32 Å in INT1and 1.58 Å in TS2). In the meantime, the hydrogen bond $N^{\varepsilon}-H^{\gamma}\cdots O^{\gamma}$ involving the transferring proton (H^{γ}) and the O^{γ} atom of Ser198 becomes progressively weaker ($R_{O\gamma-H\gamma}$ is 1.92 Å in INT1 and 2.52 Å in TS2), which is reasonable because the transferring proton (H^{γ}) is about to be transferred to the leaving ester oxygen (O2) in the current reaction step.

Step 3: Nucleophilic Attack on the Carbonyl Carbon by a Water Molecule. The choline was removed from the above-discussed QM/MM-optimized geometry of INT2 to construct the structure of INT2′, which was then relaxed by performing MD simulation. A water molecule close to the carbonyl carbon (C1) of the substrate was selected as the nucleophile and was treated by the QM method. Similarly to that in the acylation stage, the carbonyl oxygen of the substrate is also stabilized by the oxyanion hole. As shown in Figure 3B, two strong hydrogen bonds are formed between the carbonyl oxygen (O1) of ACh and the oxyanion hole in INT2′.

The current nucleophilic attacking process involves the breaking of the O^{ω}-H^{ω} bond and the formation of both $C1-O^{\omega}$ and $N^{\varepsilon}-H^{\omega}$ bonds (see Figure 3A). Thus, the distances $R_{O\omega-H\omega}$, $R_{C1-O\omega}$, and $R_{N\varepsilon-H\omega}$ were chosen to establish the reaction coordinate as $R_{O\omega-H\omega} - R_{C1-O\omega} + R_{N\varepsilon-H\omega}$ for the current reaction step. In proceeding from INT2′ to INT3 through the transition state TS3 (Figure 3), the coplanar geometry changes into tetrahedral, centering on the sp^3-hybridized carbonyl carbon (C1) atom as the nucleophilic water gradually approaches the C1 atom with a spontaneous proton (H^{ω}) transfer from the O^{ω} atom of the nucleophilic water to the N^{ε} atom of the His438 side chain. The QM/MM-optimized geometry of INT3 shows that the nucleophilic attack process is completed, with water dissociating into a hydroxide ion attaching to the C1 atom and a proton (H^{ω}) attaching to the N^{ε} atom.

Step 4: Dissociation between the Acetyl Group and Ser198 of BChE. The proton transfer between the N^{ε} atom of His438 side chain and the O^{γ} atom of the Ser198 side chain and the breaking of the covalent bond $C1-O^{\gamma}$ are involved in the dissociation of the acetyl−enzyme. The changes in the distances $R_{C1-O\gamma}$, $R_{O\gamma-H\omega}$, and $R_{N\varepsilon-H\omega}$ reflect the nature of reaction step 4. Thus, the reaction coordinate for the current reaction step was expressed as $R_{C1-O\gamma} - R_{N\varepsilon-H\omega} - R_{O\gamma-H\omega}$. Reaction step 4 is similar to reaction step 2. In both reaction steps, the C−O covalent bond is broken, and one proton is transferred from the N^{ε} atom of His438 to the oxygen atom of the broken C−O covalent bond. As shown in Figure 3, during the breaking of the $C1-O^{\gamma}$ covalent bond, the distance between the O^{γ} and H^{ω} atoms becomes closer and closer, illustrating a spontaneous proton transfer from the N^{ε} atom of the His438 side chain to the O^{γ} atom of Ser198.

Energetics. Depicted in Figure 4 is the free energy profile for BChE-catalyzed hydrolysis of ACh, determined by the QM/MM-FE calculations at the MP2/6-31+G*:AMBER level, excluding the zero-point and thermal corrections for the QM subsystem. The values given in parentheses are the corresponding relative free energies, including the zero-point and thermal corrections for the QM subsystem.

As shown in Figure 4A, with the zero-point and thermal corrections for the QM subsystem, the free energy barriers calculated for the first and second reaction steps (acylation) of BChE-catalyzed hydrolysis of ACh are 10.3 and 6.1 kcal/mol, respectively. Although the free energy barrier for the first reaction step is higher than that for the second reaction step, the relative free energy of TS2 is higher than that of TS1, indicating that the calculated overall free energy barrier for the acylation is the free energy change from ES to TS2, which is 13.8 kcal/mol. Similarly, in the deacylation stage of the BChE-catalyzed hydrolysis of ACh, the free energy barrier (9.1 kcal/mol) calculated for the third reaction step is higher than that (4.5 kcal/mol) calculated for the fourth reaction step, but the relative free energy of TS4 is higher than that of TS3, implying that the calculated overall free energy barrier for the deacylation is the free energy change from INT2′ to TS4, which is 11.9 kcal/mol. Apparently, the acylation stage with the overall free energy barrier of 13.8 kcal/mol, which is the free energy change from ES to TS2, is rate-determining for BChE-catalyzed hydrolysis of ACh.

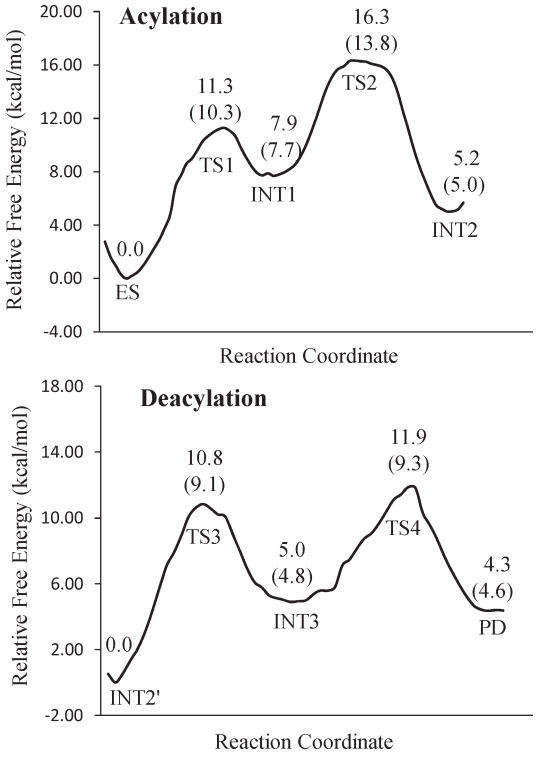

Figure 4. Free energy profiles for the acylation and deacylation stages of BChE-catalyzed hydrolysis of ACh. The relative free energies were determined by the QM/MM-FE calculations at the MP2/6-31+G*:AMBER level, excluding the zero-point and thermal corrections for the QM system. Values in the parentheses are relative free energies, including the zero-point and thermal corrections for the QM subsystem.

As mentioned above, the overall architecture of BChE structure is quite similar to that of the AChE structure. In particular, the catalytic residues in the active site gorge of both enzymes are identical. Hence, it is surprising to note that the mechanism for the BChE-catalyzed hydrolysis of ACh, in which the acylation is rate-determining, is remarkably different from the well-known mechanism for the AChE-catalyzed hydrolysis of ACh, in which the deacylation is rate-determining.[37] The mechanistic difference between BChE and AChE helps to better understand available the experimental kinetic data in the literature. In particular, it has been known that[37] the catalytic rate constant (k_{cat}) for the AChE-catalyzed hydrolysis of ACh is identical to that for the AChE-catalyzed hydrolysis of acetylthiocholine (ATCh) within the experimental errors, due to the fact that AChE-catalyzed hydrolyses of ACh and ATCh share a common rate-determining deacylation stage.

The molecular geometry of ATCh is essentially the same as that of ACh because the only structural difference between the two substrates is that the ester oxygen (O) in ACh is replaced by a sulfur (S) atom in ATCh. The experimental catalytic rate constants for BChE-catalyzed hydrolyses of ACh and ATCh have also been reported in the literature: $k_{cat} = 6.12 \times 10^4$ min^{-1} for BChE-catalyzed hydrolysis of ACh[56] and $k_{cat} = 2.02 \times 10^4$ min^{-1} for BChE-catalyzed hydrolysis of ATCh.[2] The two k_{cat} values are significantly different. The significant difference in k_{cat} between ACh and ATCh hydrolyses catalyzed by BChE indicates that the rate-determining step should not be the common deacylation stage, so the available experimental kinetic data are consistent with our computational prediction that the acylation is rate-determining for BChE-catalyzed hydrolysis of ACh.

In addition, according to the conventional transition state theory,[57] a rate constant of 6.12×10^4 min^{-1} (reported in ref 56) for BChE-catalyzed hydrolysis of ACh is associated with an activation free energy of 13.3 kcal/mol at room temperature (25 °C). The experimentally derived activation free energy of 13.3 kcal/mol is in good agreement with our predicted free energy barrier of 13.8 kcal/mol.

CONCLUSION

In this work, we employed a pseudobond first-principles QM/MM-FE approach to study the reaction pathway for BChE-catalyzed hydrolysis of ACh and the corresponding free energy profile. The computational results demonstrate that ACh hydrolysis catalyzed by BChE consists of two major reaction stages: acylation and deacylation of BChE. The acylation of BChE with ACh includes two reaction steps. The first reaction step is the nucleophilic attack on the carbonyl carbon of ACh by the hydroxyl oxygen of the Ser198 side chain; the second reaction step is the dissociation of the choline ester. The deacylation stage includes the nucleophilic attack of a water molecule on the carboxyl carbon of the substrate, followed by the dissociation of the carbonyl carbon of the substrate and the hydroxyl oxygen of the Ser198 side chain. The computationally determined free energy profile indicates that the acylation is rate-determining for the BChE-catalyzed hydrolysis of ACh, which is remarkably different from the well-known mechanism for AChE-catalyzed hydrolysis of ACh, in which the common deacylation stage is rate-determining. The computational prediction is consistent with available experimental kinetic data showing that the catalytic rate constants for BChE-catalyzed hydrolyses of ACh and ATCh are significantly different. The calculated overall free energy barrier of 13.8 kcal/mol for BChE-catalyzed hydrolysis of ACh is in good agreement with the experimentally derived activation free energy of 13.3 kcal/mol.

AUTHOR INFORMATION

Corresponding Author

*Corresponding author. Phone: 859-323-3943. Fax: 859-323-3575. E-mail: zhan@uky.edu.

Author Contributions

$These authors contributed equally to this work.

ACKNOWLEDGMENT

This work was supported in part by the NIH (Grants R01 DA025100 and R01 DA013930 to Zhan). Chen worked in Zhan's laboratory for this project at the University of Kentucky. The entire work was performed at the University of Kentucky. The authors also acknowledge the Center for Computational Sciences (CCS) at the University of Kentucky for supercomputing time on an IBM X-series Cluster with 340 nodes or 1360 processors.

REFERENCES

(1) Fuxreiter, M.; Warshel, A. *J. Am. Chem. Soc.* **1998,** *120* (1), 183–194.
(2) Boeck, A. T.; Schopfer, L. M.; Lockridge, O. *Biochem. Pharmacol.* **2002,** *63* (12), 2101–2110.
(3) Zhan, C. G.; Gao, D. Q. *Biophys. J.* **2005,** *89* (6), 3863–3872.
(4) Masson, P.; Froment, M. T.; Gillon, E.; Nachon, F.; Lockridge, O.; Schopfer, L. M. *FEBS J.* **2008,** *275* (10), 2617–2631.
(5) Mesulam, M. M.; Guillozet, A.; Shaw, P.; Levey, A.; Duysen, E. G.; Lockridge, O. *Neuroscience* **2002,** *110* (4), 627–639.
(6) Mesulam, M.; Guillozet, A.; Shaw, P.; Quinn, B. *Neurobiol. Disease* **2002,** *9* (1), 88–93.
(7) Millard, C. B.; Lockridge, O.; Broomfield, C. A. *Biochemistry* **1995,** *34* (49), 15925–15933.
(8) Lockridge, O.; Blong, R. M.; Masson, P.; Froment, M. T.; Millard, C. B.; Broomfield, C. A. *Biochemistry* **1997,** *36* (4), 786–795.
(9) Pan, Y. M.; Gao, D. Q.; Yang, W. C.; Cho, H.; Yang, G. F.; Tai, H. H.; Zhan, C. G. *Proc. Natl. Acad. Sci. U.S.A.* **2005,** *102* (46), 16656–16661.
(10) Zhan, C. G.; Zheng, F.; Landry, D. W. *J. Am. Chem. Soc.* **2003,** *125* (9), 2462–2474.
(11) Gao, D. Q.; Cho, H.; Yang, W. C.; Pan, Y. M.; Yang, G. F.; Tai, H. H.; Zhan, C. G. *Angew. Chem., Int. Ed.* **2006,** *45* (4), 653–657.
(12) Zheng, F.; Yang, W. C.; Ko, M. C.; Liu, J. J.; Cho, H.; Gao, D. Q.; Tong, M.; Tai, H. H.; Woods, J. H.; Zhan, C. G. *J. Am. Chem. Soc.* **2008,** *130* (36), 12148–12155.
(13) Zheng, F.; Zhan, C.-G. *J. Comput. Aided Mol. Des.* **2008,** *22* (9), 661–671.
(14) Zheng, F.; Zhan, C.-G. *Org. Biomol. Chem.* **2008,** *6* (5), 836–843.
(15) Gao, D. Q.; Zhan, C. G. *J. Phys. Chem. B* **2005,** *109* (48), 23070–23076.
(16) Zhan, C.-G. *Expert Rev. Clin. Pharmacol.* **2009,** *2* (1), 1–4.
(17) Yang, W.; Pan, Y.; Zheng, F.; Cho, H.; Tai, H.-H.; Zhan, C.-G. *Biophys. J.* **2009,** *96* (5), 1931–1938.
(18) Pan, Y. M.; Gao, D. Q.; Yang, W. C.; Cho, H.; Zhan, C. G. *J. Am. Chem. Soc.* **2007,** *129* (44), 13537–13543.
(19) Hamza, A.; Cho, H.; Tai, H.-H.; Zhan, C.-G. *J. Phys. Chem. B* **2005,** *109* (10), 4776–4782.
(20) Gao, D. Q.; Zhan, C.-G. *Proteins* **2006,** *62* (1), 99–110.
(21) Yang, W.; Xue, L.; Fang, L.; Chen, X.; Zhan, C.-G. *Chem.-Biol. Interact.* **2010,** *187* (1−3), 148–152.
(22) Yang, W.; Pan, Y.; Fang, L.; Gao, D.; Zheng, F.; Zhan, C.-G. *J. Phys. Chem. B* **2010,** *114* (33), 10889–10896.
(23) Brimijoin, S.; Gao, Y.; Anker, J. J.; Gliddon, L. A.; LaFleur, D.; Shah, R.; Zhao, Q. H.; Singh, M.; Carroll, M. E. *Neuropsychopharmacology* **2008,** *33* (11), 2715–2725.
(24) Decker, M. *Eur. J. Med. Chem.* **2005,** *40* (3), 305–313.
(25) Sussman, J. L.; Harel, M.; Frolow, F.; Oefner, C.; Goldman, A.; Toker, L.; Silman, I. *Science* **1991,** *253* (5022), 872–879.
(26) Saxena, A.; Redman, A. M. G.; Jiang, X. L.; Lockridge, O.; Doctor, B. P. *Biochemistry* **1997,** *36* (48), 14642–14651.
(27) Wlodek, S. T.; Antosiewicz, J.; Briggs, J. M. *J. Am. Chem. Soc.* **1997,** *119* (35), 8159–8165.
(28) Wang, Q. M.; Jiang, H. L.; Chen, J. Z.; Chen, K. X.; Ji, R. Y. *Int. J. Quantum Chem.* **1998,** *70* (3), 515–525.
(29) Vagedes, P.; Rabenstein, B.; Aqvist, J.; Marelius, J.; Knapp, E. W. *J. Am. Chem. Soc.* **2000,** *122* (49), 12254–12262.
(30) Zhang, Y. K.; Kua, J.; McCammon, J. A. *J. Am. Chem. Soc.* **2002,** *124* (35), 10572–10577.

(31) Manojkumar, T. K.; Cui, C. Z.; Kim, K. S. *J. Comput. Chem.* **2005,** *26* (6), 606–611.
(32) Suarez, D.; Field, M. J. *Proteins* **2005,** *59* (1), 104–117.
(33) Tachikawa, H.; Igarashi, M.; Nishihira, J.; Ishibashi, T. *J. Photochem. Photobiol., B* **2005,** *79* (1), 11–23.
(34) Sant'Anna, C. M. R.; Viana, A. D.; do Nascimento, N. M. *Bioorg. Chem.* **2006,** *34* (2), 77–89.
(35) Suarez, D.; Diaz, N.; Fontecilla-Camps, J.; Field, M. J. *Biochemistry* **2006,** *45* (24), 7529–7543.
(36) Zhou, Y.; Wang, S.; Zhang, Y. *J. Phys. Chem. B* **2010,** *114* (26), 8817–8825.
(37) Froede, H. C.; Wilson, I. B. *J. Biol. Chem.* **1984,** *259* (17), 1010–1013.
(38) Nemukhin, A. V.; Lushchekina, S. V.; Bochenkova, A. V.; Golubeva, A. A.; Varfolomeev, S. D. *J. Mol. Model.* **2008,** *14* (5), 409–416.
(39) Zhang, Y. K. *J. Chem. Phys.* **2005,** *122* (2), 024114.
(40) Zhang, Y. K.; Lee, T. S.; Yang, W. T. *J. Chem. Phys.* **1999,** *110* (1), 46–54.
(41) Hu, P.; Zhang, Y. K. *J. Am. Chem. Soc.* **2006,** *128* (4), 1272–1278.
(42) Zhang, Y. K.; Liu, H. Y.; Yang, W. T. *J. Chem. Phys.* **2000,** *112* (8), 3483–3492.
(43) Zhang, Y. K. *Theor. Chem. Acc.* **2006,** *116* (1−3), 43–50.
(44) Liu, J. J.; Hamza, A.; Zhan, C. G. *J. Am. Chem. Soc.* **2009,** *131* (33), 11964–11975.
(45) Liu, J. J.; Zhang, Y. K.; Zhan, C. G. *J. Phys. Chem. B* **2009,** *113* (50), 16226–16236.
(46) Liu, H. Y.; Zhang, Y. K.; Yang, W. T. *J. Am. Chem. Soc.* **2000,** *122* (28), 6560–6570.
(47) Poyner, R. R.; Larsen, T. M.; Wong, S. W.; Reed, G. H. *Arch. Biochem. Biophys.* **2002,** *401* (2), 155–163.
(48) Cisneros, G. A.; Wang, M.; Silinski, P.; Fitzgerald, M. C.; Yang, W. T. *Biochemistry* **2004,** *43* (22), 6885–6892.
(49) Metanis, N.; Brik, A.; Dawson, P. E.; Keinan, E. *J. Am. Chem. Soc.* **2004,** *126* (40), 12726–12727.
(50) Nicolet, Y.; Lockridge, O.; Masson, P.; Fontecilla-Camps, J. C.; Nachon, F. *J. Biol. Chem.* **2003,** *278* (42), 41141–41147.
(51) Frisch, M. J.; Trucks, G. W.; Schlegel, H. B.; Scuseria, G. E.; Robb, M. A.; Cheeseman, J. R.; Montgomery, J. A., Jr.; Vreven, T.; Kudin, K. N.; Burant, J. C.; Millam, J. M.; Iyengar, S. S.; Tomasi, J.; Barone, V.; Mennucci, B.; Cossi, M.; Scalmani, G.; Rega, N.; Petersson, G. A.; Nakatsuji, H.; Hada, M.; Ehara, M.; Toyota, K.; Fukuda, R.; Hasegawa, J.; Ishida, M.; Nakajima, T.; Honda, Y.; Kitao, O.; Nakai, H.; Klene, M.; Li, X.; Knox, J. E.; Hratchian, H. P.; Cross, J. B.; Bakken, V.; Adamo, C.; Jaramillo, J.; Gomperts, R.; Stratmann, R. E.; Yazyev, O.; Austin, A. J.; Cammi, R.; Pomelli, C.; Ochterski, J. W.; Ayala, P. Y.; Morokuma, K.; Voth, G. A.; Salvador, P.; Dannenberg, J. J.; Zakrzewski, V. G.; Dapprich, S.; Daniels, A. D.; Strain, M. C.; Farkas, O.; Malick, D. K.; Rabuck, A. D.; Raghavachari, K.; Foresman, J. B.; Ortiz, J. V.; Cui, Q.; Baboul, A. G.; Clifford, S.; Cioslowski, J.; Stefanov, B. B.; Liu, G.; Liashenko, A.; Piskorz, P.; Komaromi, I.; Martin, R. L.; Fox, D. J.; Keith, T.; Al-Laham, M. A.; Peng, C. Y.; Nanayakkara, A.; Challacombe, M.; Gill, P. M. W.; Johnson, B.; Chen, W.; Wong, M. W.; Gonzalez, C.; Pople, J. A. *Gaussian 03*, Revision C.02; Gaussian, Inc.: Wallingford, CT, 2004.
(52) Cieplak, P.; Cornell, W. D.; Bayly, C.; Kollman, P. A. *J. Comput. Chem.* **1995,** *16* (11), 1357–1377.
(53) Bayly, C. I.; Cieplak, P.; Cornell, W. D.; Kollman, P. A. *J. Phys. Chem.* **1993,** *97* (40), 10269–10280.
(54) Jorgensen, W. L.; Chandrasekhar, J.; Madura, J. D.; Impey, R. W.; Klein, M. L. *J. Chem. Phys.* **1983,** *79* (2), 926–935.
(55) Case, D. A.; Darden, T. A.; Cheatham, T. E. I.; Simmerling, C. L.; Wang, J.; Duke, R. E.; Luo, R.; Merz, K. M.; Wang, B.; Pearlman, D. A.; Crowley, M.; Brozell, S.; Tsui, V.; Gohlke, H.; Mongan, J.; Hornak, V.; Cui, G.; Beroza, P.; Schafmeister, C.; Caldwell, J. W.; Ross, W. S.; Kollman, P. A. *AMBER8*; University of California: San Francisco, 2004.
(56) Gao, Y.; LaFleur, D.; Shah, R.; Zhao, Q. H.; Singh, M.; Brimijoin, S. *Chem. Biol. Interact.* **2008,** *175* (1−3), 83–87.
(57) Alvarez-Idaboy, J. R.; Galano, A.; Bravo-Perez, G.; Ruiz, M. E. *J. Am. Chem. Soc.* **2001,** *123* (34), 8387–8395.